Journal of Computational and Applied Mathematics 235 (2011) 5367–5379

Contents lists available at ScienceDirect

Journal of Computational and Applied Mathematics

journal homepage: www.elsevier.com/locate/cam

Numerical simulation of fluid–structure interaction problems on hybrid meshes with algebraic multigrid methods

Huidong Yang [a,*], Walter Zulehner [b]

[a] Austrian Academy of Sciences, Johann Radon Institute for Computational and Applied Mathematics, Altenberger Strasse 69, A-4040 Linz, Austria

[b] Institute of Computational Mathematics, Johannes Kepler University Linz, Altenberger Strasse 69, 4040 Linz, Austria

ARTICLE INFO

Article history:
Received 28 January 2011

MSC:
65N30
65N55
74F10

Keywords:
Fluid–structure interaction
Partitioned approach
Hybrid meshes
Algebraic multigrid methods

ABSTRACT

Fluid–structure interaction problems arise in many fields of application such as flows around elastic structures and blood flow in arteries. The method presented in this paper for solving such a problem is based on a reduction to an equation at the interface, involving the so-called Steklov–Poincaré operators. This interface equation is solved by a Newton iteration, for which directional derivatives involving shape derivatives with respect to the interface perturbation have to be evaluated appropriately. One step of the Newton iteration requires the solution of several decoupled linear sub-problems in the structure and the fluid domains. These sub-problems are spatially discretized by a finite element method on hybrid meshes. For the time discretization, implicit first-order methods are used for both sub-problems. The discretized equations are solved by algebraic multigrid methods.

1. Introduction

A classical field of application of fluid–structure interaction (FSI) problems is aero-elasticity. Recently, FSI simulations have also been successfully used in the life sciences, in particular in hemodynamics. For instance, blood flow in the large arteries is among the most interesting and challenging applications in this area; see [1,2] and the references therein. Two main strategies for solving FSI problems have been studied: the monolithic and the partitioned approach; see, e.g., [3,1]. In this work, we adopt the second approach for solving the coupled problem, which allows the reuse of existing codes for the fluid and structure fields and requires robust solvers for the structure and the fluid sub-problems. We focus on algebraic multigrid (AMG) methods (see [4–7]) for solving both sub-problems. In this paper the sub-problems are discretized by a finite element method on hybrid meshes, which contain four element types: tetrahedron, hexahedron, prism and pyramid. In order to make the AMG methods applicable to both sub-problems, we firstly extend the standard P_1 linear element, well-known for pure tetrahedral meshes, to a macro-element on hybrid meshes. Then the AMG solvers for both sub-problems are specially adapted. In particular, for the fluid problem, we are able to construct a stabilized P_1–P_1 hierarchy on hybrid meshes; see [8].

The remainder of this paper is organized in the following way. Sections 2 and 3 follow the approach of [1] for setting up the so-called interface equation of the FSI problem and its Newton solver. In Section 4 the extended P_1 element for both sub-problems is described and analyzed. Section 5 deals with the AMG solvers for both sub-problems, and finally, in Section 6 a few numerical results are presented.

* Corresponding author.
E-mail address: huidong.yang@oeaw.ac.at (H. Yang).

0377-0427/$ – see front matter © 2011 Elsevier B.V. All rights reserved.
doi:10.1016/j.cam.2011.05.046

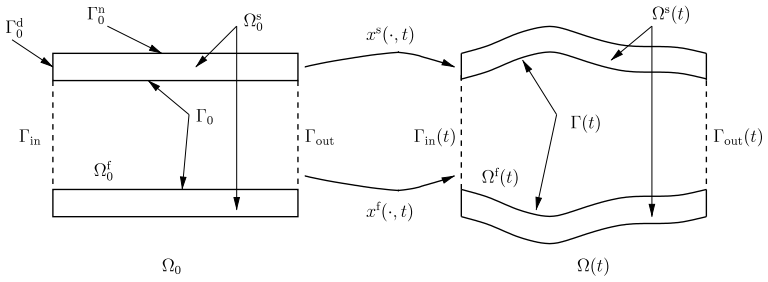

Fig. 1. The ALE mapping x.

2. Problem setting for the fluid–structure interaction

Here, we follow the approach presented in [1] and use an arbitrary Lagrangian Eulerian (ALE) formulation for the fluid and a purely Lagrangian framework for the structure.

2.1. The geometrical description and the ALE mapping

Let Ω_0 denote the initial domain at time $t = 0$ consisting of the structure and fluid sub-domains Ω_0^{s} and Ω_0^{f}, respectively. Γ_0^{d} and Γ_0^{n} denote the boundaries of the structure domain with Dirichlet and Neumann boundary conditions, respectively. Γ_0 is the initial interface between the two sub-domains. The domain $\Omega(t)$ at time t is composed of the deformable structure sub-domain $\Omega^{\mathrm{s}}(t)$ and the fluid sub-domain $\Omega^{\mathrm{f}}(t)$. $\Gamma_{\mathrm{in}}(t)$ and $\Gamma_{\mathrm{out}}(t)$ denote the boundaries of the fluid domain with inflow and outflow boundary conditions, respectively. The corresponding interface $\Gamma(t)$ is evolving from the initial interface Γ_0. The evolution of $\Omega(t)$ is obtained by an injective mapping (Fig. 1):

$$x\colon \Omega_0 \times \mathbb{R}_+ \longrightarrow \mathbb{R}^3.$$

The position of a point $x_0 \in \Omega_0^{\mathrm{s}}$ at time t is given by the mapping for the structure domain

$$x_t^{\mathrm{s}} : \Omega_0^{\mathrm{s}} \to \Omega^{\mathrm{s}}(t)$$

with $x_t^{\mathrm{s}}(x_0) \equiv x^{\mathrm{s}}(x_0, t) = x(x_0, t) = x_0 + d^{\mathrm{s}}(x_0, t)$ for $x_0 \in \Omega_0^{\mathrm{s}}$, where $d^{\mathrm{s}}(x_0, t)$ denotes the displacement of the structure domain at time t.

Correspondingly, the position of a point $x_0 \in \Omega_0^{\mathrm{f}}$ at time t is given by the ALE mapping for the fluid domain

$$x_t^{\mathrm{f}} : \Omega_0^{\mathrm{f}} \to \Omega^{\mathrm{f}}(t)$$

with $x_t^{\mathrm{f}}(x_0) \equiv x^{\mathrm{f}}(x_0, t) = x(x_0, t) = x_0 + d^{\mathrm{f}}(x_0, t)$ for $x_0 \in \Omega_0^{\mathrm{f}}$, where $d^{\mathrm{f}}(x_0, t)$ denotes the displacement in the fluid domain at time t.

The displacement d^{f} is typically defined as an extension of the structure displacement d^{s} at the interface Γ_0:

$$d^{\mathrm{f}} = \mathrm{Ext}(d^{\mathrm{s}}|_{\Gamma_0}).$$

Here we follow the classical approach and use the harmonic extension. The displacement $d^{\mathrm{f}} = d^{\mathrm{f}}(x_0, t)$ is the solution of the boundary value problem

$$\begin{aligned} -\Delta d^{\mathrm{f}} &= 0 \quad && \text{in } \Omega_0^{\mathrm{f}}, \\ d^{\mathrm{f}} &= 0 && \text{on } \Gamma_{\mathrm{in}} \cup \Gamma_{\mathrm{out}}, \\ d^{\mathrm{f}} &= d^{\mathrm{s}} && \text{on } \Gamma_0. \end{aligned} \tag{1}$$

Furthermore, we introduce the domain velocities

$$w^{\mathrm{s}} = \frac{\partial x^{\mathrm{s}}}{\partial t} = \frac{\partial d^{\mathrm{s}}}{\partial t} \quad \text{and} \quad w^{\mathrm{f}} = \frac{\partial x^{\mathrm{f}}}{\partial t} \circ \left(x_t^{\mathrm{f}}\right)^{-1} = \frac{\partial d^{\mathrm{f}}}{\partial t} \circ \left(x_t^{\mathrm{f}}\right)^{-1}$$

for the structure and fluid domain, respectively.

2.2. The physical model in strong form

We start by describing the models used for the structure and the fluid domain.

2.2.1. Structure modeling

For the structure problem we use the pure displacement formulation in the Lagrangian framework, defined on the reference material configuration Ω_0^{s}. The state variable d^{s} satisfies the balance law of momentum

$$\rho_{\mathrm{s}} \frac{\partial^2 d^{\mathrm{s}}}{\partial t^2} - \mathrm{div}\sigma_{\mathrm{s}}(d^{\mathrm{s}}) = f_{\mathrm{s}} \quad \text{in } \Omega_0^{\mathrm{s}}, \tag{2}$$

and the boundary conditions

$$\begin{aligned} d^{\mathrm{s}} &= 0 && \text{on } \Gamma_0^{\mathrm{d}}, \\ \sigma_{\mathrm{s}}(d^{\mathrm{s}})n_{\mathrm{s}} &= 0 && \text{on } \Gamma_0^{\mathrm{n}}, \end{aligned} \tag{3}$$

where ρ_{s} is the density, σ_{s} is the first Piola–Kirchhoff stress tensor, f_{s} the external force density, and n_{s} the outward normal of Ω_0^{s}.

In particular, we use the linear Saint Venant–Kirchhoff elastic model:

$$\sigma_{\mathrm{s}}(d^{\mathrm{s}}) = 2\mu^l \varepsilon(d^{\mathrm{s}}) + \lambda^l \operatorname{div}(d^{\mathrm{s}})I, \qquad \varepsilon(d^{\mathrm{s}}) = \frac{1}{2}\left(\nabla d^{\mathrm{s}} + (\nabla d^{\mathrm{s}})^T\right)$$

with Lamé constants λ^l and μ^l.

2.2.2. Fluid modeling

For the fluid problem we use the incompressible Navier–Stokes equations in the Eulerian framework:

$$\rho_{\mathrm{f}} \frac{\partial u}{\partial t} + \rho_{\mathrm{f}}(u \cdot \nabla)u - 2\mu \operatorname{div} \varepsilon(u) + \nabla p = 0 \quad \text{in } \Omega^{\mathrm{f}}(t), \tag{4}$$

$$\operatorname{div} u = 0 \quad \text{in } \Omega^{\mathrm{f}}(t) \tag{5}$$

with boundary conditions

$$\begin{aligned} \sigma_{\mathrm{f}}(u,p)n_{\mathrm{f}} &= g_{\mathrm{in}} && \text{on } \Gamma_{\mathrm{in}}(t), \\ \sigma_{\mathrm{f}}(u,p)n_{\mathrm{f}} &= 0 && \text{on } \Gamma_{\mathrm{out}}(t), \end{aligned} \tag{6}$$

where ρ_{f} denotes the fluid density, μ the dynamic viscosity, and

$$\sigma_{\mathrm{f}}(u,p) = -pI + 2\mu\varepsilon(u), \qquad \varepsilon(u) = \frac{1}{2}\left(\nabla u + (\nabla u)^{\mathrm{T}}\right),$$

for the Cauchy stress tensor σ_{f} and the strain rate tensor ε, respectively.

The ALE time derivative of u is introduced in order to overcome the difficulty for evaluating the time derivative of velocity u under the Eulerian framework in a moving domain. The ALE time derivative is given by

$$\left.\frac{\partial u}{\partial t}\right|_{x_0} = \frac{\partial}{\partial t}\left(u \circ x_t^{\mathrm{f}}\right) \circ \left(x_t^{\mathrm{f}}\right)^{-1} = \frac{\partial u}{\partial t} + (w^{\mathrm{f}} \cdot \nabla)u.$$

Using this, we obtain the ALE formulation of (4):

$$\rho_{\mathrm{f}} \left.\frac{\partial u}{\partial t}\right|_{x_0} + \rho_{\mathrm{f}}\left((u - w^{\mathrm{f}}) \cdot \nabla\right)u - 2\mu \operatorname{div} \varepsilon(u) + \nabla p = 0 \quad \text{in } \Omega^{\mathrm{f}}(t). \tag{7}$$

2.2.3. Interface conditions

When coupling the two sub-problems together, interface conditions are needed. In particular, no-slip conditions at the interface Γ_0 are explicitly imposed on Γ_0 between the structure and the fluid domain:

$$u \circ x_t^{\mathrm{f}} = \frac{\partial d^{\mathrm{s}}}{\partial t} \quad \text{on } \Gamma_0. \tag{8}$$

The second interface condition is the equilibrium of normal stresses:

$$(\sigma_{\mathrm{f}}(u,p)n_{\mathrm{f}}) \circ x_t^{\mathrm{f}} + \sigma_{\mathrm{s}}(d^{\mathrm{s}})n_{\mathrm{s}} = 0 \quad \text{on } \Gamma_0. \tag{9}$$

To summarize, the complete model consists of problem (1), Eqs. (2), (5) and (7), boundary conditions (3) and (6), and interface conditions (8) and (9) for the state variables d^{s}, d^{f}, u, p, and λ, complemented with prescribed initial values for d^{s}, $w^{\mathrm{s}} = \partial d^{\mathrm{s}}/\partial t$, and u.

2.2.4. Reformulation of the model

As in [1], we introduce the interface variable $\lambda = \lambda(t)$ on Γ_0 at time t by using

$$\lambda = d^{\mathrm{s}}|_{\Gamma_0} = d^{\mathrm{f}}|_{\Gamma_0}.$$

Let $S_{\mathrm{s}}(\lambda)$ denote the Neumann data of the structure problem with prescribed Dirichlet data λ at the interface Γ_0, i.e.,

$$S_{\mathrm{s}}(\lambda) := \sigma_{\mathrm{s}}(d^{\mathrm{s}})n_{\mathrm{s}},$$

where the displacement $d^s = d^s(x_0, t)$ solves the structure problem

$$\begin{aligned}
&\rho_s \frac{\partial^2 d^s}{\partial t^2} - \operatorname{div}(\sigma_s(d^s)) = f_s && \text{in } \Omega_0^s,\\
&\sigma_s(d^s) n_s = 0 && \text{on } \Gamma_0^n,\\
&d^s = 0 && \text{on } \Gamma_0^d,\\
&d^s = \lambda && \text{on } \Gamma_0
\end{aligned}$$

with the prescribed initial values for d^s and $w^s = \partial d^s/\partial t$.

Let $S_f(\lambda)$ denote the Neumann data of the fluid problem with prescribed Dirichlet data $\partial\lambda(t)/\partial t$ at the interface Γ_0, i.e.,

$$S_f(\lambda) := (\sigma_f(u, p) n_f) \circ x_t^f,$$

where u and p solve the fluid problem

$$\begin{aligned}
&\rho_f \left.\frac{\partial u}{\partial t}\right|_{x_0} + \rho_f \left((u - w^f)\cdot\nabla\right) u - 2\mu \operatorname{div} \varepsilon(u) + \nabla p = 0 && \text{in } \Omega^f(t),\\
&\operatorname{div} u = 0 && \text{in } \Omega^f(t),\\
&\sigma_f(u, p) n_f = g_{in} && \text{on } \Gamma_{in}(t),\\
&\sigma_f(u, p) n_f = 0 && \text{on } \Gamma_{out}(t),\\
&u \circ x_t^f = \frac{\partial \lambda}{\partial t} && \text{on } \Gamma_0
\end{aligned}$$

with the prescribed initial value for u. The fluid domain is given by

$$\Omega^f(t) = \left(id + d^f\right)(\Omega_0^f),$$

where id denotes the identity operator and $d^f = d^f(x_0, t)$ is the harmonic extension of λ:

$$\begin{aligned}
&-\Delta d^f = 0 && \text{in } \Omega_0^f,\\
&d^f = 0 && \text{on } \Gamma_{in} \cup \Gamma_{out}\\
&d^f = \lambda && \text{on } \Gamma_0.
\end{aligned}$$

With these notations the coupled problem reduces to the following equation:

$$S_s(\lambda) + S_f(\lambda) = 0 \quad \text{on } \Gamma_0 \text{ for each time } t.$$

The mappings S_s and S_f are called Steklov–Poincaré operators.

2.3. Weak formulations and time discretization

Let $H^1(\Omega_0^s)$, $H^1(\Omega_0^f)$ and $L^2(\Omega_0^f)$ denote the standard Sobolev and Lebesgue spaces on Ω_0^s and Ω_0^f, respectively.

2.3.1. The weak formulation of the structure problem

By standard techniques, we obtain the following weak formulation of the structure sub-problem in $V^s = \{v^s \in H^1(\Omega_0^s)^3 : v^s = 0 \text{ on } \Gamma_0^d\}$: Find $d^s = d^s(t) \in V_\lambda^s(t) = \{v^s \in V^s : v^s = \lambda(t) \text{ on } \Gamma_0\}$ such that

$$\int_{\Omega_0^s} \rho_s \frac{\partial^2 d^s}{\partial t^2} \cdot v^s dx + \int_{\Omega_0^s} [\lambda^l \operatorname{div} d^s \operatorname{div} v^s + 2\mu^l \varepsilon(d^s) : \varepsilon(v^s)] dx = 0$$

for all $v^s \in V_0^s = \{v^s \in V^s : v^s = 0 \text{ on } \Gamma_0\}$.

2.3.2. Time discretization of the structure problem

For the time discretization of the structure sub-problem, we follow the strategy in [1] and use a Newmark method with $\gamma = 2\beta = 1$. Let $d^{s,n}$ and $w^{s,n}$ denote the approximations of the displacement and the structure domain velocity at time t^n, respectively. Then, for the displacement at the next time level $t^{n+1} = t^n + \delta t$, the following variational problem must be solved: Find $d^{s,n+1} \in V_\lambda^s(t^{n+1})$ such that

$$a^s(d^{s,n+1}, v^s) = \langle F^s, v^s \rangle \quad \text{for all } v^s \in V_0^s \tag{10}$$

with the bilinear and linear forms

$$\begin{aligned}
a^s(d^s, v^s) &= \frac{2}{\delta t^2} \int_{\Omega_0^s} \rho_s d^s v^s dx + \int_{\Omega_0^s} [\lambda^l \operatorname{div} d^s \operatorname{div} v^s + 2\mu^l \varepsilon(d^s) : \varepsilon(v^s)] dx,\\
\langle F^s, v^s \rangle &= \frac{2}{\delta t^2} \int_{\Omega_0^s} \rho_s (d^{s,n} + \delta t\, w^{s,n}) v^s dx.
\end{aligned}$$

The structure domain velocity at the next time level is then given by

$$w^{s,n+1} = \frac{2}{\delta t}(d^{s,n+1} - d^{s,n}) - w^{s,n}.$$

2.3.3. The weak formulation of the fluid problem

The harmonic extension leads to the following weak formulation in $D^{\mathrm{f}} = \{d^{\mathrm{f}} \in H^1(\Omega_0^{\mathrm{f}})^3 : d^{\mathrm{f}} = 0 \text{ on } \Gamma_{\mathrm{in}} \cup \Gamma_{\mathrm{out}}\}$: Find $d^{\mathrm{f}} = d^{\mathrm{f}}(t) \in D_\lambda^{\mathrm{f}}(t) = \{d \in D^{\mathrm{f}} : d = \lambda(t) \text{ on } \Gamma_0\}$ such that

$$\int_{\Omega_0^{\mathrm{f}}} \nabla d^{\mathrm{f}} : \nabla \phi \mathrm{d}x = 0 \quad \text{for all } \phi \in D_0^{\mathrm{f}} = \{d \in D^{\mathrm{f}} : d = 0 \text{ on } \Gamma_0\}.$$

For the fluid problem we obtain the following weak formulation in $V^{\mathrm{f}}(t) = \{v^{\mathrm{f}} : v^{\mathrm{f}} \circ x_t^{\mathrm{f}} \in H^1(\Omega_0^{\mathrm{f}})^3\}$ and $Q^{\mathrm{f}}(t) = \{q^{\mathrm{f}} : q^{\mathrm{f}} \circ x_t^{\mathrm{f}} \in L^2(\Omega_0^{\mathrm{f}})\}$: Find $u = u(t) \in V_\lambda^{\mathrm{f}}(t) = \{v^{\mathrm{f}} \in V^{\mathrm{f}}(t) : v^{\mathrm{f}} \circ x_t^{\mathrm{f}} = \partial\lambda/\partial t(t) \text{ on } \Gamma_0\}$ and $p = p(t) \in Q^{\mathrm{f}}(t)$ such that

$$\begin{aligned}
&\frac{\mathrm{d}}{\mathrm{d}t} \int_{\Omega^{\mathrm{f}}(t)} \rho_{\mathrm{f}} u \cdot v^{\mathrm{f}} \mathrm{d}x - \int_{\Omega^{\mathrm{f}}(t)} \rho_{\mathrm{f}} \mathrm{div}\, w^{\mathrm{f}} u \cdot v^{\mathrm{f}} \mathrm{d}x + \int_{\Omega^{\mathrm{f}}(t)} \rho_{\mathrm{f}} \left((u - w^{\mathrm{f}}) \cdot \nabla\right) u \cdot v^{\mathrm{f}} \mathrm{d}x \\
&\quad + 2\mu \int_{\Omega^{\mathrm{f}}(t)} \varepsilon(u) : \varepsilon(v^{\mathrm{f}}) \mathrm{d}x - \int_{\Omega^{\mathrm{f}}(t)} p \,\mathrm{div}\, v^{\mathrm{f}} \mathrm{d}x = \int_{\Gamma_{\mathrm{in}}(t)} g_{\mathrm{in}} \cdot v^{\mathrm{f}} \mathrm{d}s, \\
&\quad - \int_{\Omega^{\mathrm{f}}(t)} q^{\mathrm{f}} \,\mathrm{div}\, u \mathrm{d}x = 0
\end{aligned}$$

for all $v^{\mathrm{f}} \in V_0^{\mathrm{f}}(t) = \{v^{\mathrm{f}} \in V^{\mathrm{f}}(t) : v^{\mathrm{f}} \circ x_t^{\mathrm{f}} = 0 \text{ on } \Gamma_0\}$ and $q^{\mathrm{f}} \in Q^{\mathrm{f}}(t)$.

2.3.4. Time discretization of the fluid problem

Firstly, we compute the harmonic extension at the new time t^{n+1}: Find $d^{\mathrm{f},n+1} \in D_\lambda^{\mathrm{f}}(t^{n+1})$ such that

$$\int_{\Omega_0^{\mathrm{f}}} \nabla d^{\mathrm{f},n+1} : \nabla \phi \mathrm{d}x = 0 \quad \text{for all } \phi \in D_0^{\mathrm{f}}. \tag{11}$$

Then the fluid domain $\Omega^{\mathrm{f}}(t^{n+1})$ at t^{n+1} is obtained from

$$\Omega^{\mathrm{f}}(t^{n+1}) = (\mathrm{i}d + d^{\mathrm{f},n+1})(\Omega_0^{\mathrm{f}})$$

and we set for the fluid domain velocity

$$w^{\mathrm{f},n+1} = \frac{1}{\delta t}(d^{\mathrm{f},n+1} - d^{\mathrm{f},n}) \circ \left(x_{t^{n+1}}^{\mathrm{f}}\right)^{-1}.$$

For the time discretization of the Navier–Stokes equations an implicit Euler scheme is used. The non-linear convective term is treated in a semi-implicit way; see [2]. Let u^n denote the approximation of the velocity at time t^n. Then we obtain the following mixed variational problem: Find $(u^{n+1}, p^{n+1}) \in V_\lambda^{\mathrm{f}}(t^{n+1}) \times Q^{\mathrm{f}}(t^{n+1})$ such that

$$\begin{aligned}
&a^{\mathrm{f}}(u^{n+1}, v^{\mathrm{f}}) + b^{\mathrm{f}}(v^{\mathrm{f}}, p^{n+1}) = \langle F^{\mathrm{f}}, v^{\mathrm{f}} \rangle, \\
&b^{\mathrm{f}}(u^{n+1}, q^{\mathrm{f}}) = 0
\end{aligned} \tag{12}$$

for all $(v^{\mathrm{f}}, q^{\mathrm{f}}) \in V_0^{\mathrm{f}}(t^{n+1}) \times Q^{\mathrm{f}}(t^{n+1})$, with the bilinear and linear forms

$$\begin{aligned}
a^{\mathrm{f}}(u, v^{\mathrm{f}}) \;=\; & \frac{1}{\delta t} \int_{\Omega^{\mathrm{f}}(t^{n+1})} \rho_{\mathrm{f}} u \cdot v^{\mathrm{f}} \mathrm{d}x - \int_{\Omega^{\mathrm{f}}(t^{n+1})} \rho_{\mathrm{f}} \left(\mathrm{div}\, w^{\mathrm{f},n+1}\right) u \cdot v^{\mathrm{f}} \mathrm{d}x \\
& + \int_{\Omega^{\mathrm{f}}(t^{n+1})} \rho_{\mathrm{f}} \left(\left(\hat{u}^n - w^{\mathrm{f},n+1}\right) \cdot \nabla\right) u \cdot v^{\mathrm{f}} \mathrm{d}x \\
& + 2\mu \int_{\Omega^{\mathrm{f}}(t^{n+1})} \varepsilon(u) : \varepsilon(v^{\mathrm{f}}) \mathrm{d}x,
\end{aligned} \tag{13}$$

$$b^{\mathrm{f}}(v^{\mathrm{f}}, q^{\mathrm{f}}) = -\int_{\Omega^{\mathrm{f}}(t^{n+1})} q^{\mathrm{f}} \,\mathrm{div}\, v^{\mathrm{f}} \mathrm{d}x,$$

$$\langle F^{\mathrm{f}}, v^{\mathrm{f}} \rangle = \frac{1}{\delta t} \int_{\Omega^{\mathrm{f}}(t^n)} \rho_{\mathrm{f}} u^n \cdot \hat{v}^{\mathrm{f}} \mathrm{d}x + \int_{\Gamma_{\mathrm{in}}(t^{n+1})} g_{\mathrm{in}} \cdot v^{\mathrm{f}} \mathrm{d}s,$$

where $\hat{u}^n = u^n \circ x_{t^n}^{\mathrm{f}} \circ (x_{t^{n+1}}^{\mathrm{f}})^{-1}$ and $\hat{v}^{\mathrm{f}} = v^{\mathrm{f}} \circ x_{t^{n+1}}^{\mathrm{f}} \circ \left(x_{t^n}^{\mathrm{f}}\right)^{-1}$.

2.3.5. The weak formulation of the interface equation

Let $H^{1/2}(\Gamma_0)$ denote the trace space of V_s, i.e., $H^{1/2}(\Gamma_0) = \{v_s|_{\Gamma_0} : v_s \in V_s\}$, and let $H^{-1/2}(\Gamma_0)$ be the dual space of $H^{1/2}(\Gamma_0)$.

In the time-discretized weak formulation, the Steklov–Poincaré operators S_{s} and S_{f} become operators which map the Dirichlet data on the interface, i.e. the displacement $\lambda = d^{\mathrm{s},n+1} = d^{\mathrm{f},n+1} \in H^{1/2}(\Gamma_0)^3$, to the corresponding Neumann

data on the interface, i.e. the normal stresses, $\sigma_s(d^{s,n+1})n_s$ and $\sigma_f(u^{n+1}, p^{n+1})n_f \circ (\mathrm{id} + d^{s,n+1}) \in H^{-1/2}(\Gamma_0)^3$, where $d^{s,n+1}$ solves the structure problem (10) for given initial values $d^{s,n}$ and $w^{s,n}$, and $d^{f,n+1}$, u^{n+1}, p^{n+1} solve problem (11) and the fluid problem (12) for given initial values u^n.

More precisely, for the structure sub-problem and the fluid sub-problem, the Steklov–Poincaré operators are given by

$$\langle S_s(\lambda), \mu\rangle_{\Gamma_0} = a^s(d^{s,n+1}, v^s) - \langle F^s, v^s\rangle$$
$$\langle S_f(\lambda), \mu\rangle_{\Gamma_0} = a^f(u^{n+1}, v^f) + b(v^f, p^{n+1}) - \langle F^f, v^f\rangle$$

for all $\mu \in H^{1/2}(\Gamma_0)^3$ and all $v^s \in V^s$, $v^f \in V^f(t)$ with $\mu = v^s = v^f \circ x_t^f$ on Γ_0.

Then we end up with the following problem for each time step: Find $\lambda^{n+1} \in H^{1/2}(\Gamma_0)^3$ such that

$$\langle S_f(\lambda^{n+1}), \mu\rangle_{\Gamma_0} + \langle S_s(\lambda^{n+1}), \mu\rangle_{\Gamma_0} = 0 \quad \text{for all } \mu \in H^{1/2}(\Gamma_0)^3. \tag{14}$$

3. Newton's method for the interface equation

3.1. Newton's method

In each time step $t^{n+1} = t^n + \delta t$ the interface equation (14) must be solved. For simplicity we will drop the superscript $n+1$ from now on for the remaining part of the section. So the problem now reads (in operator notation)

$$S_s(\lambda) + S_f(\lambda) = 0.$$

Newton's method applied to the interface equation is given by

$$\lambda_{k+1} = \lambda_k - \left(S_s'(\lambda_k) + S_f'(\lambda_k)\right)^{-1} \left(S_s(\lambda_k) + S_f(\lambda_k)\right),$$

where subscript k indicates the Newton iteration steps; see [1]. In each step of the iterative method a problem of the form

$$\left(S_s'(\lambda_k) + S_f'(\lambda_k)\right) \delta\lambda_k = -\left(S_s(\lambda_k) + S_f(\lambda_k)\right)$$

has to be solved. For this we will use (after discretization in space; see Section 4) a preconditioned GMRES method with preconditioner $S_s'(\lambda_k)$ (see [1]).

See Algorithm 1 for a schematic description of the computational method.

Algorithm 1 Newton's method for the interface equation.

For $k \geq 0$,

1: compute the residual $S_s(\lambda_k) + S_f(\lambda_k)$ by solving the structure and fluid sub-problems,
2: solve the linear problem $\left(S_s'(\lambda_k) + S_f'(\lambda_k)\right) \delta\lambda_k = -\left(S_s(\lambda_k) + S_f(\lambda_k)\right)$ via a preconditioned GMRES method,
3: update the displacement $\lambda_{k+1} = \lambda_k + \delta\lambda_k$, and if not accurate enough, go to step 1.

Note that Step 1 can be parallelized due to the independence of the sub-problems for given λ_k. Step 2 requires solving linearized structure and fluid problems several times during the GMRES iteration. An AMG method will be used for this; see Section 5.

This algorithm requires the evaluation of $S_s(\lambda)$, $S_f(\lambda)$ by solving the structure and fluid sub-problems, and the evaluation of $S_s'(\lambda)\delta\lambda$, $S_f'(\lambda)\delta\lambda$, which we will briefly discuss next; for details see [8].

3.2. Evaluation of $S_s'(\lambda)\delta\lambda$

For the directional derivative of $S_s(\lambda)$ in direction $\delta\lambda$ one easily obtains

$$\langle S_s'(\lambda)\delta\lambda, \mu\rangle_{\Gamma_0} = a^s(\delta d^s, v^s)$$

for all $\mu \in H^{1/2}(\Gamma_0)$ and all $v^s \in V^s$ with $\mu = v^s$ on Γ_0, where $\delta d^s \in V^s_{\delta\lambda} = \{v^s \in D^s : v^s = \delta\lambda \text{ on } \Gamma_0\}$ solves the structure problem with modified right hand side

$$a^s(\delta d^s, v) = 0 \quad \text{for all } v \in V_0^s. \tag{15}$$

3.3. Evaluation of $S_f'(\lambda)\delta\lambda$

For the directional derivative of $S_f(\lambda)$ in direction $\delta\lambda$ one obtains after some calculations

$$\langle S_f'(\lambda)\delta\lambda, \mu\rangle_{\Gamma_0} = a^f(\delta u, v^f) + b(v^f, \delta p) - \langle \tilde{F}^f, v^f\rangle$$

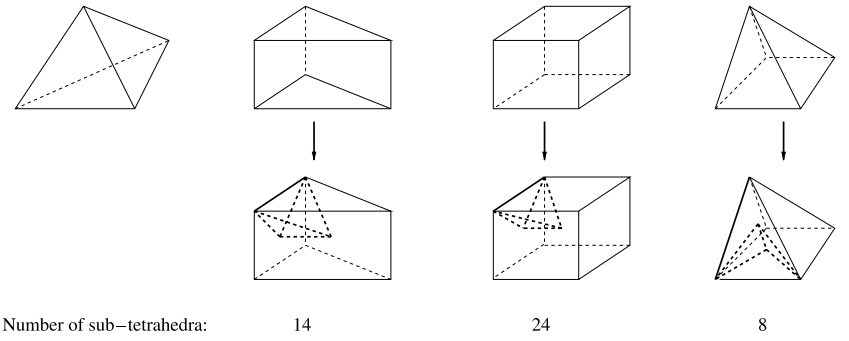

Fig. 2. Splitting of element domains into tetrahedra.

for all $\mu \in H^{1/2}(\Gamma_0)$ and all $v^{\mathrm{f}} \in V^{\mathrm{f}}(t)$ with $\mu = v^{\mathrm{f}} \circ x_t^{\mathrm{f}}$ on Γ_0, where the linear functional $\tilde{F}^{\mathrm{f}}$ is given by

$$\begin{aligned}\langle \tilde{F}^{\mathrm{f}}, v^{\mathrm{f}} \rangle = {} & \frac{1}{\delta t} \int_{\Omega^{\mathrm{f}}(t)} \rho_{\mathrm{f}} \left(\delta\hat{d}^{\mathrm{f}} \cdot \nabla \right) u \cdot v^{\mathrm{f}} \mathrm{d}x + \int_{\Omega^{\mathrm{f}}(t)} \rho_{\mathrm{f}} \left(\mathrm{div} \left(\left(I \, \mathrm{div}\, \delta\hat{d}^{\mathrm{f}} - \nabla\delta\hat{d}^{\mathrm{f}} \right) w \right) \right) u \cdot v^{\mathrm{f}} \mathrm{d}x \\ & - \int_{\Omega^{\mathrm{f}}(t)} \rho_{\mathrm{f}} \left(\hat{u}^n - w \right) \cdot \nabla u \left(I \, \mathrm{div}\, \delta\hat{d}^{\mathrm{f}} - \nabla\delta\hat{d}^{\mathrm{f}} \right) \cdot v^{\mathrm{f}} \mathrm{d}x + \mu \int_{\Omega^{\mathrm{f}}(t)} \left(\nabla u \nabla\delta\hat{d}^{\mathrm{f}} + \left(\nabla u \nabla\delta\hat{d}^{\mathrm{f}} \right)^T \right) : \nabla v^{\mathrm{f}} \mathrm{d}x \\ & - 2\mu \int_{\Omega^{\mathrm{f}}(t)} \varepsilon(u) \left(I \, \mathrm{div}\, \delta\hat{d}^{\mathrm{f}} - \left(\nabla\delta\hat{d}^{\mathrm{f}} \right)^T \right) : \nabla v^{\mathrm{f}} \mathrm{d}x + \int_{\Omega^{\mathrm{f}}(t)} p \left(I \, \mathrm{div}\, \delta\hat{d}^{\mathrm{f}} - \left(\nabla\delta\hat{d}^{\mathrm{f}} \right)^T \right) : \nabla v^{\mathrm{f}} \mathrm{d}x\end{aligned}$$

with $\delta\hat{d}^{\mathrm{f}} = \delta d^{\mathrm{f}} \circ (\mathrm{id} + d^{\mathrm{f}})^{-1}$ and the directional derivatives δu, δp and δd^{f} of $u(\lambda)$, $p(\lambda)$ and $d^{\mathrm{f}}(\lambda)$ in direction $\delta\lambda$. The directional derivative δd^{f} is given by

$$\delta d^{\mathrm{f}} = \mathrm{Ext}(\delta\lambda).$$

The directional derivatives $\delta u \in \{v \in V^{\mathrm{f}}(t) : \delta u \circ (\mathrm{id} + d^{\mathrm{f}}) = \delta d^{\mathrm{f}}/\delta t \text{ on } \Gamma_0\}$ and $\delta p \in Q^{\mathrm{f}}(t)$ are given as the solution of the modified fluid mixed problem:

$$\begin{aligned} & a^{\mathrm{f}}(\delta u, v^{\mathrm{f}}) + b(v^{\mathrm{f}}, \delta p) = \langle \tilde{F}^{\mathrm{f}}, v^{\mathrm{f}} \rangle, \\ & b(\delta u, q) = \langle \tilde{G}^{\mathrm{f}}, q \rangle \end{aligned} \tag{16}$$

for all $v^{\mathrm{f}} \in V_0^{\mathrm{f}}(t)$, $q \in Q^{\mathrm{f}}(t)$ with

$$\langle \tilde{G}, q \rangle = - \int_{\Omega^{\mathrm{f}}(t)} q \, \mathrm{div} \left(\left(I \, \mathrm{div}\, \delta\hat{d}^{\mathrm{f}} - \nabla\delta\hat{d}^{\mathrm{f}} \right) u \right) \mathrm{d}x.$$

4. Finite element discretization on a hybrid mesh

The spatial discretization was done by a finite element method. In fluid–structure interaction problems it is quite standard that the underlying mesh is composed of different element domains such as tetrahedra, hexahedra, pyramids and prisms. We call such meshes hybrid meshes and we will describe next how the classical conforming P_1 finite element on purely tetrahedral meshes can be extended to such hybrid meshes.

We assume that $\mathcal{M}_h$ is an admissible subdivision of a computational domain Ω into polyhedral element domains, i.e. any two elements from $\mathcal{M}_h$ either have no intersection, or have a common face, or have a common edge, or have a common vertex. For defining the extended P_1 finite element on $\mathcal{M}_h$ we first need a refined mesh. Each non-tetrahedral element domain M is subdivided into a number of tetrahedra in the following way: for each non-triangular face of M we introduce a node at the center of the face and connect this node with all vertices of M lying on that face. This results in subdividing each non-triangular face into several triangles. Then we add another node at the center of M and connect this node with all vertices and all face centers. By this means the polyhedron M is eventually subdivided into several tetrahedra, e.g., a prism is split into 14 tetrahedra, a hexahedron into 24 tetrahedra, and a pyramid into 8 tetrahedra; see Fig. 2 for an illustration.

One easily sees that the resulting tetrahedral subdivision $\mathcal{T}_h$ is an admissible refinement of the original hybrid mesh $\mathcal{M}_h$.

4.1. The extended P_1 element on a hybrid mesh

The shape functions of the P_1 element on a tetrahedron T are the polynomials of degree ≤ 1; the degrees of freedom are the values at the vertices of the tetrahedron. A possible extension of this element to a general polyhedron M can be done in the following way. We first consider the conforming P_1 element on the underlying subdivision of M into tetrahedra as described above, whose degrees of freedom are the values at the vertices of M and at all additionally introduced nodes at face and element centers. Then we eliminate the extra degrees of freedom at the center of a face by the averaging of the values

at the vertices of the face, and, analogously, we eliminate the extra degree of freedom at the center of M by the averaging of the values at the vertices of M. So we end up with a finite element whose shape functions are continuous and piecewise linear in the underlying tetrahedral subdivision and whose degrees of freedom are the values at the vertices of the original undivided element domains. We call this finite element the extended P_1 element on a hybrid mesh.

It is easy to construct a nodal basis for the extended P_1 element on $\mathcal{M}_h$. Let x be a vertex of an element domain from $\mathcal{M}_h$, let $x_{F,i}$, $i = 1, \ldots,$ denote the center of those non-triangular faces F_i which contain x as a vertex, and let $x_{M,j}$, $j = 1, \ldots,$ denote the center of those domains elements M_j which contain x as a vertex. Then the nodal basis function φ associated with the vertex x is given by

$$\varphi = \hat{\varphi} + \sum_i \frac{1}{N_{F,i}} \hat{\varphi}_{F,i} + \sum_j \frac{1}{N_{M,j}} \hat{\varphi}_{M,j},$$

where $\hat{\varphi}$, $\hat{\varphi}_{F,i}$, and $\hat{\varphi}_{F,i}$ denote the nodal basis functions of the P_1 element on $\mathcal{T}_{\hat{h}}$ associated with the nodes x, $x_{F,i}$ and $x_{M,j}$, respectively, and $N_{F,i}$ and $N_{M,j}$ are the numbers of vertices of the face F_i and the element domain M_j, respectively.

The extended P_1 element on hybrid meshes is an $H^1(\Omega)$-conforming finite element and has similar approximation properties to the (standard) P_1 element on tetrahedral meshes. Under standard assumptions, the following approximation properties were shown for the corresponding finite element space V_h; for details see [8]:

Theorem 1. 1. *There is an interpolation operator $I_C: L^2(\Omega) \longrightarrow V_h$ such that*

$$\|v - I_C v\|_{L^2(\Omega)} \le c|v|_{L^2(\Omega)} \quad \text{for all } v \in L^2(\Omega),$$

and

$$\|v - I_C v\|_{L^2(\Omega)} + h|v - I_C v|_{H^1(\Omega)} \le ch|v|_{H^1(\Omega)} \quad \text{for all } v \in H^1(\Omega)$$

with a mesh-independent constant c.

2. *There is an interpolation operator $I_L: H^2(\Omega) \longrightarrow V_h$ such that*

$$\|v - I_L v\|_{L^2(\Omega)} + h|v - I_L v|_{H^1(\Omega)} \le ch^2|v|_{H^2(\Omega)} \quad \text{for all } v \in H^1(\Omega)$$

with a mesh-independent constant c.

The operator I_C is a Clément-type interpolation operator; the operator I_L is a Lagrange-type interpolation operator.

4.2. The extended P_1 element for the structure and the fluid sub-problems

We assume that the computational domains Ω_0^s and Ω_0^f are discretized by a hybrid mesh with matching vertices at the interface Γ_0.

The extended P_1 element on the hybrid mesh restricted to the structure domain Ω_0^s was used to discretize the variational problems (10) and (15) for computing approximations to the displacement $d^{s,n+1}$ and the directional derivative δd^s. The approximation to the structure domain velocity $w^{s,n+1}$ is then set analogously to that for the continuous case.

The extended P_1 element on the hybrid mesh restricted to the fluid domain Ω_0^f was used to discretize the harmonic extension problem for computing an approximation of the displacement $d^{f,n+1}$ and the directional derivative δd^f. The next computational domain $\Omega^f(t^{n+1})$ and the corresponding fluid domain velocity are then set analogously to the continuous case.

Special care is required if the extended P_1 element is used for discretizing velocity as well as pressure in the fluid problems (12) and (16) on the fluid domain $\Omega^f(t^{n+1})$. Finite element methods for fluid problems with equal order approximations for both velocity and pressure spaces usually suffer from two possible sources of instability. One source is a dominating advection term, and the other source is a possible violation of the discrete inf – sup stability condition for the velocity and pressure approximations.

The first problem can be overcome by the well-known *streamline upwind Petrov–Galerkin (SUPG) method* (see [9]), in which the momentum equation is tested with elementwise modified test functions. The other problem can be treated by using the *pressure-stabilization Petrov–Galerkin (PSPG)* method introduced in [10]. Both problems can be resolved by a unified approach with element test functions which take into account both *SUPG* and *PSPG*; see [11]. We followed exactly this approach with the same choice of the stabilization parameters as in [11] applied to the tetrahedral refinement of the original hybrid mesh; see [8] for details.

5. Algebraic multigrid methods for the structure and fluid sub-problems

After discretization in time and space, linear systems for sub-problems arise at each time step.

The variational problems on the structure domain and the harmonic extension problems on the fluid domain are symmetric and coercive. The discretized problems lead to linear systems with symmetric and positive definite matrices. Algebraic multigrid methods for solving such problems are well-studied; see, e.g., [4] for scalar differential equations and [12] for an extension to systems of partial differential equations in a natural blockwise fashion (blockwise interpolation). The particular AMG method used in our experiments was taken from [7].

The situation is more subtle for mixed variational problems like the fluid problems. They are not coercive. Therefore, the discretized problems do not automatically inherit the stability properties of the original problems. This leads to a major problem for AMG methods. They are based on a hierarchy of linear systems derived for the original discretized problem by some coarsening strategy. We have to make sure that we do not lose stability by coarsening. The basic approach that we propose is discussed in the next subsection. For simplicity we will present the basic idea for the Stokes problem only. The extension of the technique to the more general fluid sub-problems that we have to face in fluid–structure interaction problems is straightforward.

5.1. The AMG for the Stokes problem

Here we followed closely the work by Markus Wabro (see [6,13,14]), and extended it to problems arising from a stabilized finite element discretization on hybrid meshes (see [8] for more details).

The saddle point problem arising from the discretized Stokes problem is given by

$$K\begin{pmatrix} u \\ p \end{pmatrix} = \begin{pmatrix} f \\ g \end{pmatrix}, \quad \text{with} \quad K = \begin{pmatrix} A & B^T \\ B & -C \end{pmatrix}, \tag{17}$$

where A is symmetric and positive definite, B has full rank, and C is symmetric and positive semi-definite. The matrix C results from the pressure stabilization. Then the (negative) Schur complement

$$S = BA^{-1}B^T + C$$

is symmetric and positive definite.

The AMG method requires an appropriate coarsening strategy and a smoothing procedure. We first address the coarsening strategy.

5.2. The coarsening strategy

One important feature of the AMG method for the coupled problem is to coarsen the velocity and pressure unknowns separately. If one applies the coarsening strategy to the whole system in a straightforward way, it will lead to a mixture of velocity and pressure components on coarse levels.

For the prolongation from the coarser level $l+1$ to the next finer level l we choose a matrix of the form

$$P_{l+1}^l = \begin{pmatrix} \tilde{I}_{l+1}^l & \\ & J_{l+1}^l \end{pmatrix} \quad \text{with} \quad \tilde{I}_{l+1}^l = \begin{pmatrix} I_{l+1}^l & & \\ & I_{l+1}^l & \\ & & I_{l+1}^l \end{pmatrix}.$$

The prolongation matrices, interpreted as operators

$$I_{l+1}^l : \mathbb{R}^{n_{l+1}} \to \mathbb{R}^{n_l} \quad \text{and} \quad J_{l+1}^l : \mathbb{R}^{m_{l+1}} \to \mathbb{R}^{m_l},$$

are defined for one velocity component and pressure, respectively. For the general mixed element, these two prolongation matrices may be chosen differently. In our case, where we use the same extended P_1 element for the velocity components and the pressure, it is natural to choose $J_{l+1}^l = I_{l+1}^l$. In particular, we used the coarsening strategy of the AMG method from [7] applied to one of the three identical diagonal blocks of A.

For the restriction from the finer level l to the next coarser level $l+1$ we choose the transposed matrix:

$$R_l^{l+1} = (P_{l+1}^l)^T.$$

The system matrix on the level l is denoted by K_l and has the form

$$K_l = \begin{pmatrix} A_l & B_l^T \\ B_l & -C_l \end{pmatrix}.$$

A standard procedure for constructing the matrix on the next coarser level $l+1$ is the Galerkin projection method:

$$K_{l+1} = R_l^{l+1} K_l P_{l+1}^l = \begin{pmatrix} A_{l+1} & B_{l+1}^T \\ B_{l+1} & -C_{l+1} \end{pmatrix}$$

with

$$A_{l+1} = I_l^{l+1} A_l I_{l+1}^l, \qquad B_{l+1} = J_l^{l+1} B_l I_{l+1}^l, \qquad C_{l+1} = J_l^{l+1} C_l J_{l+1}^l.$$

Since the matrix C involves mesh-dependent stabilization parameters, the usage of the Galerkin projection for C_{l+1} results in a loss of stability on coarser levels. Therefore, the Galerkin method is only used for the coarsening of A and B, while a different strategy was applied for coarsening C: we set

$$C_{l+1} = \frac{1}{h^2} \lambda_{\max}(D_l^{-1} M_l) \tilde{C}_{l+1},$$

where $\tilde{C}_{l+1}$ denotes the standard Galerkin projection of C, h is the mesh size of the finest mesh, M_l is the mass matrix on level l obtained by Galerkin projection, and D_l denotes the diagonal of A_l.

Under appropriate assumptions on the hybrid mesh the following stability result was shown; see [8]:

Theorem 2. *For each level l, there is a constant* $\zeta_l > 0$ *such that*

$$\sup_{0\neq(v,q)\in V_l\times Q_l} \frac{\mathcal{B}_l((u,p),(v,q))}{\|v\|_{A_l}+\|q\|_{M_l}} \geq \zeta_l \left(\|u\|_{A_l}+\|p\|_{M_l}\right)$$

for all $(u,p)\in V_l\times Q_l = (\mathbb{R}^{n_l})^3\times\mathbb{R}^{m_l}$, *where*

$$\mathcal{B}_l((u,p),(v,q)) = v^T A_l u + v^T B_l^T p + q^T B_l u - q^T C_l p.$$

5.3. The smoothing procedure

As the smoothing procedure a Braess–Sarazin-type smoother was used. This smoother was originally introduced in [15] and has a smoothing property with a rate of $\mathcal{O}(1/m)$, where m is the number of smoothing steps.

The smoothing procedure is a preconditioned Richardson method:

$$\begin{pmatrix} u_{k+1}\\ p_{k+1}\end{pmatrix} = \begin{pmatrix} u_k\\ p_k\end{pmatrix} + \hat{K}^{-1}\begin{pmatrix} f - Au_k - B^T p_k\\ g - Bu_k + Cp_k\end{pmatrix}$$

with preconditioner

$$\hat{K} = \begin{pmatrix} \hat{A} & B^T\\ B & \hat{A}^{-1}B^T - \hat{S}\end{pmatrix},$$

where $\hat{A}$ and $\hat{S}$ are symmetric and positive definite preconditioners for A and the (negative) inexact Schur complement $C + B\hat{A}^{-1}B^T$, respectively.

One step of the method requires us to solve the following three equations consecutively:

$$\begin{aligned}\hat{A}(\hat{u}_{k+1} - u_k) &= f - Au_k - B^T p_k,\\ \hat{S}(p_{k+1} - p_k) &= B\hat{u}_{k+1} - Cp_k - g,\\ \hat{A}(u_{k+1} - u_k) &= -B^T(p_{k+1} - p_k).\end{aligned}$$

As suggested in [6], we use $\hat{A} = 2D$, where D denotes the diagonal of A. The choice $\hat{S} = C + B^T\hat{A}^{-1}B$ corresponds to the original Braess–Sarazin smoother. It requires the (exact) solution of the equation

$$(C + B^T\hat{A}^{-1}B)(p_{k+1} - p_k) = B\hat{u}_{k+1} - Cp_k - g.$$

We use instead one step of an (inner) AMG method with starting value 0 to solve this equation approximately. See [16] for an analysis of such an approximate Braess–Sarazin smoother.

6. Numerical results

Numerical experiments are reported for the example of a straight cylindrical vessel taken from [1]. The fluid domain at rest is a cylinder in the z-direction of length 5 cm and radius 5 mm at rest. The thickness of the surrounding structure is 0.5 mm.

The structure is a linear Saint Venant–Kirchhoff material with density $\rho^s = 1.2$ and Lamé constants $\mu^l = 1.15\times 10^6$ and $\lambda^l = 1.73\times 10^6$ with no acting body forces.

The fluid has density $\rho^f = 1.0$ and viscosity $\mu = 0.03$. For the fluid, we set the Neumann data $g_{\text{in}}(t) = (0, 0, 1.332\times 10^4)^T$ dyn/cm^2 on the inlet for $t \leq 3$ ms and $g_{\text{in}}(t) = 0$ afterwards.

The fluid and structure are initially at rest.

Two meshes are used for simulations; see Fig. 3.

The coarse mesh contains 4176 vertices and 3965 elements (1944 structure elements and 2021 fluid elements), and the fine mesh 17,904 vertices and 17,489 elements (7434 structure elements and 10,055 fluid elements). The overall degrees of freedom for these two meshes are about 16,000 and 70,000, respectively.

We use different time step sizes $\delta t = 0.25, 0.125, 0.0625$ ms and run the simulation until the time $t = 10$ ms on the coarse mesh. The pressure waves along the center line are compared for these three time step sizes in Fig. 4. A further refinement leads to a time step size $\delta t = 0.03125$ ms. The corresponding pressure waves are almost identical to the results with a time step size $\delta t = 0.0625$ ms. So, obviously, convergence with respect to the temporal discretization has been observed.

Fig. 5 compares the pressure waves along the center line of the cylinder on the coarse mesh and on the fine mesh. The results for the two meshes are almost identical, except that the speed of the wave on the fine mesh is a little bit faster than that on the coarse one. So, to some extent, convergence with respect to the spatial discretization has also been observed.

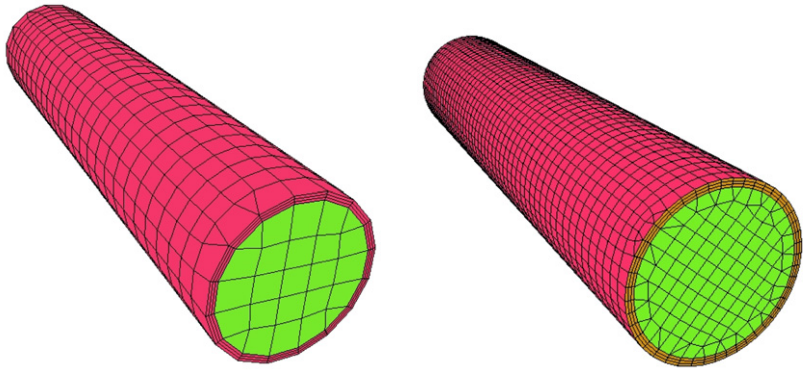

(a) Coarse mesh. (b) Fine mesh.

Fig. 3. Fine and coarse meshes for simulations.

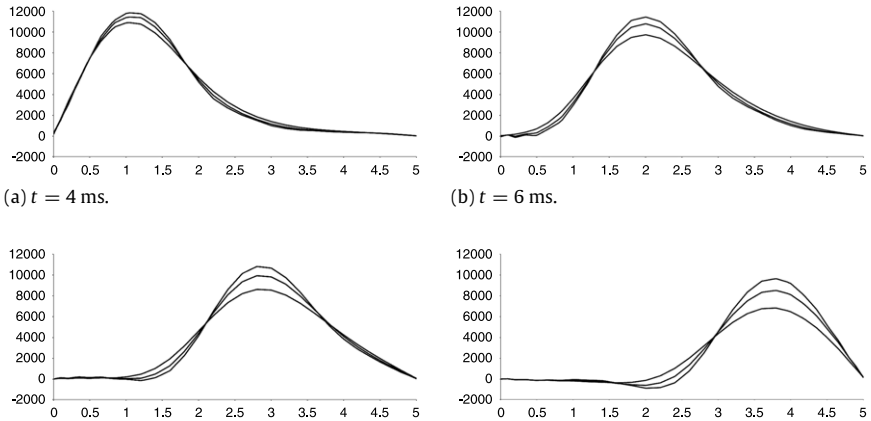

(a) $t = 4$ ms. (b) $t = 6$ ms.

(c) $t = 8$ ms. (d) $t = 10$ ms.

Fig. 4. Pressure waves at different time levels with three different time step sizes: $\delta t = 0.25, 0.125, 0.0625$ ms. The horizontal axis represents the center line of the cylinder; the pressure is plotted in the vertical direction.

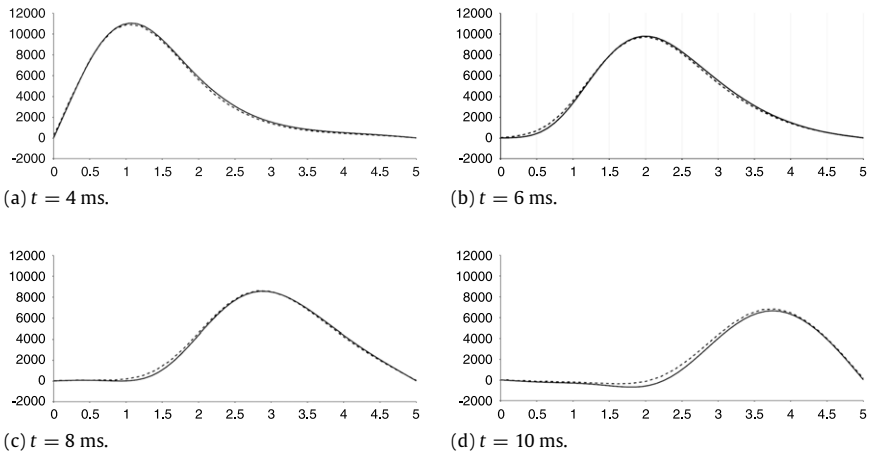

(a) $t = 4$ ms. (b) $t = 6$ ms.

(c) $t = 8$ ms. (d) $t = 10$ ms.

Fig. 5. Pressure waves at different time levels with a time step size $\delta t = 0.25$ ms, on two meshes: a fine mesh (solid lines) and a coarse mesh (dashed lines). The horizontal axis represents the center line of the cylinder; the pressure is plotted in the vertical direction.

We plot the pressure wave as a function of time t, at the center point of the cylinder; see Fig. 6. It is observed that the pressure wave reaches its maximal value approximately at 7 ms.

Fig. 7 shows the deformation of the computational structure domain on the coarse mesh at different time levels. For visualization purposes, the deformation is amplified by a factor of 12. The results are comparable to those given in [1].

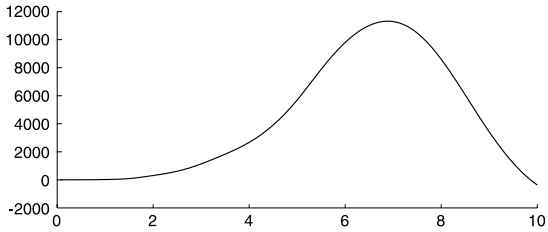

Fig. 6. The pressure wave as a function of time at the center point, with a time step size $\delta t = 0.0625$ ms. The horizontal axis is the time axis; the pressure is plotted in the vertical direction.

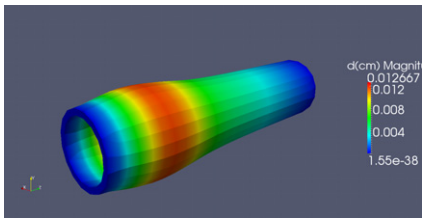

(a) $t = 4$ ms.

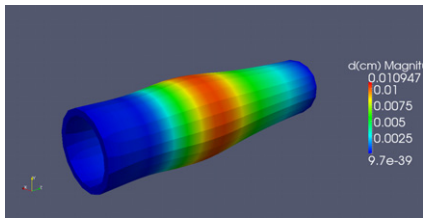

(b) $t = 6$ ms.

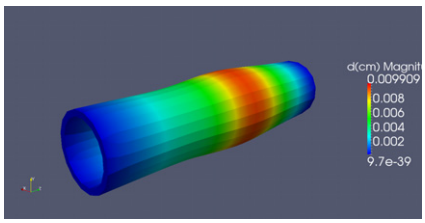

(c) $t = 8$ ms.

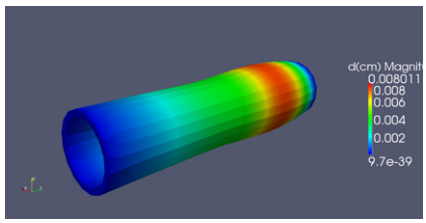

(d) $t = 10$ ms.

Fig. 7. Visualization of deformed structure domains at different time levels.

As regards the iteration numbers, we have observed the following results. A relative error reduction by a factor of 10^{-5} is achieved in 2–3 outer Newton iterations; each of these iterations requires 6–8 GMRES iterations for a relative residual error reduction by a factor of 10^{-5}. For solving the structure problem, about 10 preconditioned conjugate gradient iterations with AMG preconditioning are needed for a relative residual error reduction by a factor of 10^{-10}; for the fluid problem about 5 AMG iterations for a relative residual error reduction by a factor of 10^{-10}. Almost the same numbers of iterations were observed for the coarse and fine meshes.

The code is tested on a laptop with an Intel Core of 2.0 GHz and 1 GB memory. For a time step size $\delta t = 0.25$ ms, we run the simulation until $t = 10$ ms, for problems on both coarse and fine meshes. The overall running time is about two days on the coarse mesh, and about two weeks on the fine mesh. There is still some work to do related to the optimization of our FSI code in order to achieve better performance.

Acknowledgments

This work was supported by the Austrian Grid, a project funded by the Federal Ministry of Science and Research, and, in part, by the Austrian Science Fund (FWF) under grant W1214/DK12.

References

[1] S. Deparis, M. Discacciati, G. Fourestey, A. Quarteroni, Fluid–structure algorithms based on Steklov–Poincaré operators, Comput. Methods Appl. Mech. Engrg. 195 (2006) 5797–5812.
[2] M.A. Fernández, M. Moubachir, A Newton method using exact Jacobians for solving fluid–structure coupling, Comput. Struct. 83 (2–3) (2005) 127–142.
[3] M. Heil, An efficient solver for the fully coupled solution of large-displacement fluid–structure interaction problems, Comput. Methods Appl. Mech. Engrg. 193 (1–2) (2004) 1–23.
[4] J.W. Ruge, K. Stüben, Algebraische mehrgittermethodenalgebraic multigrid (AMG), in: Multigrid Methods, in: Frontiers in Applied Mathematics, vol. 3, SIAM, Philadelphia, 1987, pp. 73–130.
[5] S. Reitzinger, Algebraic multigrid methods for large scale finite element equations, Ph.D. Thesis, Johannes Kepler University Linz, 2001.
[6] M. Wabro, Algebraic multigrid methods for the numerical solution of the incompressible Navier–Stokes equations, Ph.D. Thesis, Johannes Kepler University Linz, 2003.
[7] F. Kickinger, Algebraic multigrid for discrete elliptic second-order problems, in: W. Hackbush (Ed.), Multigrid Methods V. Proceedings of the 5th European Multigrid Conference, in: Lecture Notes in Computational Sciences and Engineering, vol. 3, Springer, 1998, pp. 157–172.

[8] H. Yang, Numerical simulations of fluid–structure interaction problems on hybrid meshes with algebraic multigrid methods, Ph.D. Thesis, Johannes Kepler University Linz, 2010.
[9] A.N. Brooks, T.J.R. Hughes, Streamline upwind/Petrov–Galerkin formulation for convection dominated flows with particular emphasis on the incompressible Navier–Stokes equations, Comput. Methods Appl. Mech. Engrg. 32 (1982) 199–259.
[10] T.J.R. Hughes, L.P. Franca, M.A. Balestra, A new finite element formulation for computational fluid dynamics: V. Circumventing the Babuška-Brezzi condition: a stable Petrov–Galerkin formulation of the Stokes problem accommodating equal order interpolations, Comput. Methods Appl. Mech. Engrg. 59 (1986) 85–99.
[11] M. Braack, E. Burman, V. John, G. Lube, Stabilized finite element methods for the generalized *O* seen problem, Comput. Methods Appl. Mech. Engrg. 196 (2007) 853–866.
[12] M. Griebel, D. Oeltz, M.A. Schweitzer, An algebraic multigrid method for linear elasticity, SIAM J. Sci. Comput. 25 (2003) 385–407.
[13] M. Wabro, Coupled algebraic multigrid methods for the Oseen problem, Comput. Vis. Sci. 7 (2004) 141–151.
[14] M. Wabro, AMGe—coarsening strategies and application to the *O* seen equations, SIAM J. Sci. Comput. 27 (2006) 2077–2097.
[15] D. Braess, R. Sarazin, An efficient smoother for the Stokes problem, Appl. Numer. Math. 23 (1997) 3–19.
[16] W. Zulehner, A class of smoothers for saddle point problems, Computing 65 (2000) 227–246.